



Mafic injection as a trigger for felsic magmatism: A numerical study

M. Schubert

Department of Earth Sciences, Institute of Geochemistry and Petrology, ETH Zurich, Clausiusstrasse 25, 8092 Zurich, Switzerland (maike.schubert@erdw.ethz.ch)

T. Driesner

Department of Earth Sciences, Institute of Geochemistry and Petrology, ETH Zurich, Zurich, Switzerland

T. V. Gerya

Department of Earth Sciences, Institute of Geophysics, ETH Zurich, Zurich, Switzerland

P. Ulmer

Department of Earth Sciences, Institute of Geochemistry and Petrology, ETH Zurich, Zurich, Switzerland

[1] The origin of crustal-scale silicic magmatism remains a matter of debate, and notable uncertainty exists concerning the physical mechanisms that drive ascent and emplacement of felsic magmas in upper crustal regions. A 2-D numerical model demonstrates that injection of mantle-derived mafic magma into a partially molten hot zone in the lower crust can drive felsic magma ascent and intrusion into upper crustal levels. The injection of mafic magma induces overpressure in the reservoir, which increases crustal stresses and triggers development of brittle/plastic shear zones, and can drive significant surface uplift. The emerging topography causes a nonuniform overpressure distribution in the reservoir and can trigger felsic magma ascent along crustal shear zones. Based on systematic numerical experiments, we investigate the influence of crustal strength and injection rate. The initial upper crustal strength controls the degree of crustal faulting and surface uplift and therefore whether felsic magma ascent can be initiated or not. The final upper crustal strength influences the depth and final style of felsic intrusion. The injection rate of mafic magma determines the time scale of overpressure growth and surface uplift stage. In contrast, the duration of the subsequent felsic ascent and intrusion emplacement stages remains nearly constant. Our results imply that mafic underplating and intrusion into the lower crust may not only be a prime control for the generation of felsic magmas in the lower crust but may also be an important physical driving mechanism for felsic magma ascent and intrusion into upper crustal levels.

Components: 11,500 words, 7 figures, 3 tables.

Keywords: numerical modeling; magma emplacement; felsic magmatism; pluton formation.

Index Terms: 0545 Computational Geophysics: Modeling (1952, 4255, 4316); 0545 Pluton emplacement: Pluton emplacement (1952, 4255, 4316); 8159 Tectonophysics: Rheology: crust and lithosphere (8031).

Received 26 October 2012; **Revised** 18 March 2013; **Accepted** 18 March 2013; **Published** 17 June 2013.

Schubert, M., T. Driesner, T. V. Gerya, and P. Ulmer (2013), Mafic injection as a trigger for felsic magmatism: A numerical study, *Goechem. Geophys. Geosyst.*, 14, 1910–1928, doi:10.1002/ggge.20124.

1. Introduction

[2] Ascent of felsic magma from the lower continental crust and its emplacement in upper crustal levels is a major process of mass and heat transfer in the crust, leading to plutonic and volcanic complexes and the formation of economic deposits of metals such as Cu, Mo, Au, Sn, and others in the upper crust [Petford *et al.*, 2000]. Accordingly, the mechanisms of felsic magma generation in the lower crust, its ascent to upper crustal levels, and its final emplacement as plutonic intrusions have been the subject of numerous studies. In spite of significant progress toward understanding these processes, they remain a subject of vivid debate and the understanding of the interactions between them are still particularly incomplete [Zellmer and Annen, 2008, and references therein].

[3] Three main mechanisms can lead to generation of felsic melt [Thompson and Connolly, 1995]: (1) H₂O supply that lowers the melting temperature of felsic rocks, (2) decompression melting, and (3) increased heat supply in parts of the lower crust. While the first two mechanisms occur under relatively specific geologic conditions, heat supply by mafic underplating is believed to be a common process that can operate in diverse setting ranging from island arcs through orogenic belts to intracontinental settings including rift zones [Annen and Sparks, 2002; Bergantz, 1989; Hildreth and Moorbath, 1988; Huppert and Sparks, 1988; Stern, 2002]. The intrusion and underplating of mafic mantle magma can lead to “hot zones” in the lower crust, in which both the differentiation of mafic magma and partial melting of crustal material near the mafic intrusion can contribute to the generation of significant amounts of felsic melt [Annen *et al.*, 2006].

[4] Evidence for correlation of mafic magma and felsic pluton formation is common. For example, at the Sierra Nevada Batholith, xenolith studies [e.g., Ducea and Saleeby, 1998; Lee *et al.*, 2001] and outcrops of tectonically displaced lower crustal parts [e.g., Pickett and Saleeby, 1993] show such a connection. A particularly relevant example is the Ivrea Zone where a large-scale system of felsic magmatism is exposed from a near-surface caldera structure to a paleodepth of ~25 km [Sinigoi *et al.*, 2011, Quick *et al.*, 1994; Rudnick, 1990]. There, field observations and geochronological data indicate a close spatial and temporal relationship between the intrusion of mafic magma into the deep crust and resident silicic magmas that were either entirely or partly generated by lower

crustal anatexis and/or through differentiation from more primitive mantle-derived magmas [Quick *et al.*, 2009]. These authors suggested that the injection of mantle-derived magma into the deep crust may have triggered the ascent of felsic magma to upper crustal levels. To the best of our knowledge, the physics of such a process have not yet been studied.

[5] Magma generated within lower crustal levels has to find a way to ascend through the crust in order to reach the surface or form plutons in upper crustal regions. Different models of magma ascent have been suggested with diking and diapiric ascent as end-members [Brown, 2007; Olsen *et al.*, 2004]. Diking is a process in which the magma ascends along fractures that may be preexisting or initiated by the magma intrusion itself. In contrast, diapiric ascent is a purely viscous process, where buoyant, viscous magma ascends within a viscous crust. Whether diking or diapiric ascent occurs is mainly governed by the viscosity contrast between the host rock and the magma. There are different additional ascent mechanisms like stoping or zone melting [Marsh, 1982]. Stopping denotes magma ascending while melting/disintegrating the host rock. Zone melting is a process of combined magma generation and ascent. The top of the magma body melts while the floor solidifies, and therefore, a melt-body rises but the original magma is replaced with increasing degrees of melted host rock material as the process proceeds.

[6] The composite nature of many large felsic intrusions in the crust indicates that their emplacement may happen in pulses rather than as a single event [e.g., Annen and Sparks, 2002; Atherton, 1993; Horsman *et al.*, 2005; Michel *et al.*, 2008]. Annen [2011] modeled the thermal consequences of batholith formation by multiple batches of magma. She found that a critical frequency of intrusions is necessary to form one single magma chamber. In the case of a slower succession of magma batches, earlier batches have already cooled down and crystallized and the magma accumulates as individual sheets underlying one another. Torres del Paine is a well-studied field example where the construction of the batholith from different batches of magma has been identified [Leuthold *et al.*, 2012]. The total time of accretion of the Torres del Paine batholith is 90,000 years. Michel *et al.* [2008] calculated the interval between the intrusions of individual magma batches to be on the order of 10,000 years.

[7] During accumulation of large plutons, space needs to be generated within the crust [Bons *et al.*, 2004]. Acocella [2000] suggests roof lifting as one

mechanism of space accommodation for the intrusion of big plutons such as the example of the Amiata area in southern Tuscany. *Acocella and Mulugeta* [2001] provided analogue models for intrusion-driven surface uplift that shows similar overall uplift regimes to what they found in the field.

[8] The final emplacement level of intrusions in upper crustal regions is thought to depend on the interaction of rheology and rigidity contrasts within the crust, the crustal stress field, and the crustal and lithospheric density structure [e.g., *Burov et al.*, 2003; *Gerya and Burg*, 2007; *Menand*, 2011]. The influence of these parameters has been studied using analogue experiments [*Mazzarini et al.*, 2010] and further constrained by field observations and numerical studies [e.g., *Burg et al.*, 2009; *Burov*, 2003; *Gerya and Burg*, 2007; *Gudmundsson*, 2011].

[9] In this paper, we present results of 2-D numerical thermomechanical simulations that study the effects of mafic mantle magma intrusion into a lower crustal felsic magma reservoir. We restricted our study to a generic geometry in order to be able to cover a parameter space that is both computationally manageable and sufficiently large to explore the first-order physical effects of this process. We demonstrate that the process can trigger felsic melt ascent to upper crustal plutonic and volcanic levels and explore how crustal rheology and mafic inflow rate affect the results.

2. Simulation Method

[10] We used the thermomechanical numerical code (I2ELVIS) described in *Gerya and Yuen* [2007] and *Gerya* [2010] that is based on 2-D finite differences with marker in cell technique. I2ELVIS was intensively tested for different problems by comparison with analytical solutions [*Gerya and Yuen*, 2003; *Gerya and Yuen*, 2007] and analogue sandbox models [*Buiter et al.*, 2006]. We represent the crust by a visco-elasto-plastic rheology, and the magma is treated as a viscous fluid [*Pinkerton and Stevenson*, 1992].

2.1. Conservation Equations

[11] The main governing equations are the continuity equation for mass conservation [e.g., *Turcotte and Schubert*, 2002], an equation that describes energy conservation, and the 2-D equation for creeping flow (Stokes equation). A detailed discussion of the equations is given in *Gerya* [2010].

[12] The continuity equation for incompressible flows is used:

$$\nabla \cdot \vec{v} = 0 \quad (1)$$

whereby \vec{v} denotes the velocity field in x and y directions.

[13] The energy conservation equation considers heat conduction and advection and includes external heat sources like shear heating:

$$\rho C_p \left(\frac{DT}{Dt} \right) = \nabla \cdot (k \nabla T) + T \alpha (\vec{v} \cdot \nabla P) + H_r + H_s \quad (2)$$

where ρ denotes density, C_p isobaric heat capacity, and DT/Dt is the substantial time derivative of the temperature T (i.e., $DT/Dt = \partial T / \partial t + \vec{v} \cdot \nabla T$). k is the thermal conductivity, α the thermal expansion coefficient, P the pressure, and H_r and H_s are radioactive and shear heating, respectively.

[14] The 2-D Stokes equation for creeping flow is formulated in terms of the deviatoric stress tensor σ'_{ij} :

$$\frac{\partial \sigma'_{ij}}{\partial x_j} - \frac{\partial P}{\partial x_i} + \rho P_i g_i = 0 \quad (3)$$

where g_i denotes the gravitational acceleration and is zero in horizontal direction.

2.2. Melt Crystallization and Partial Melting

[15] Partial melting and crystallization of the lower crust and magmas are expressed via a simple linear approximation [*Gerya and Burg*, 2007]:

$$M = 0; \quad \text{at } T \leq T_{\text{solidus}} \\ M = \frac{T - T_{\text{solidus}}}{T_{\text{liquidus}} - T_{\text{solidus}}}; \quad \text{at } T_{\text{liquidus}} > T > T_{\text{solidus}} \\ M = 1; \quad \text{at } T > T_{\text{liquidus}} \quad (4)$$

where M refers to the melt fraction, and T_{solidus} and T_{liquidus} denote the solidus and the liquidus temperatures that are depending on the material and on the pressure. Based on the simplicity of our linear melting model and uncertainty of composition and water content for crustal and mantle magmas, we used the same T_{solidus} and T_{liquidus} for all magmas and for the lower crust in our numerical experiments (Table 1). Table 1 lists the material properties used in our simulations [*Gerya and Burg* 2007].

[16] The effective density of partially molten rocks is calculated via

$$\rho_{\text{eff}} = \rho_{\text{solid}} - M(\rho_{\text{solid}} - \rho_{\text{melt}}) \quad (5)$$

with the densities of solid rock and melt varying with temperature and pressure according to

Table 1. Physical Properties of Rocks Used in the Simulations^a

Material	ρ_0 , kg/m ³	k , W/(m K) (at T_K , P_{MPa})	$T_{solidus}$, K (at P_{MPa})	$T_{liquidus}$, K (at P_{MPa})	Q_L , kJ/kg	H_r , $\mu W/m^3$	Flow Law for Solid Rocks ^c	C_0/C_1 , MPa F_{CO}/F_{C1} , γ_0/γ_1	Shear Modulus, GPa
Sediments	2700	$[0.64 + 807/(T + 77)]$ $\times (1 + 0.00004P)$				2	wet quartzite	0.5/0.5, 0.2/ 0, 0/0.05	10
Upper crust	2700	$[0.64 + 807/(T + 77)]$ $\times (1 + 0.00004P)$				1	wet quartzite	50/8, 0/0, 0/ 0.25	25
Lower crust and felsic magma	2800 (solid) 2700 (molten)	$[1.18 + 474/(T + 77)]$ $\times (1 + 0.00004P)$	973–70,400/ ($P + 354$) + 77,800,000/ ($P + 354$) ² at $P < 1600$ MPa, 935 + 0.0035 P + 0.0000062 P^2 at $P > 1600$ MPa	1423 + 0.105 P	380	0.25	plagioclase An ₇₅	0.1/0.1, 0.2/ 0, 0/0.05	25
Mafic magma	3000 (solid) 2800 (molten)	$[1.18 + 474/(T + 77)]$ $\times (1 + 0.00004P)$	973–70,400/ ($P + 354$) + 77,800,000/ ($P + 354$) ² at $P < 1600$ MPa, 935 + 0.0035 P + 0.0000062 P^2 at $P > 1600$ MPa	1423 + 0.105 P	380	0.25	plagioclase An ₇₅	50/0.5, 0.6/ 0.6, 0/0.1	25
Lithosphere - asthenosphere mantle	3300	$[0.73 + 1293/(T + 77)]$ $\times (1 + 0.00004P)$				0.022	dry olivine	50/50, 0.6/ 0.6, 0.5/1.5	67
References^b	1, 2	3,9	4,5,6,7,8	4	1, 2	1	10	11	1

^aOther properties (for all rock types): $C_p = 1000 \text{ J kg}^{-1} \text{ K}^{-1}$, $\alpha = 3 \times 10^{-5} \text{ K}^{-1}$, and $\beta = 1 \times 10^{-11} \text{ MPa}^{-1}$.

^b1, Turcotte and Schubert [2002]; 2, Bitner and Schmelting [1995]; 3, Clauser and Huenges [1995]; 4, Schmidt and Huenges [1995]; 5, Hess [1989]; 6, Hirschmann [2000]; 7, Johannes [1985]; 8, Poli and Schmidt [2002]; 9, Hofmeister [1999]; 10, Ranalli [1995]; 11, Gerya and Burg [2007].

^cFlow law parameter from Ranalli [1995]: wet quartzite: $E(\text{kJ/mol}) = 154$, $n = 2.3$, $A_D(\text{MPa}^{-n} \text{s}^{-1}) = 10^{-3.5}$, $V(U(\text{MPa mol})) = 0$; plagioclase An₇₅: $E(\text{kJ/mol}) = 154$, $n = 2.3$, $A_D(\text{MPa}^{-n} \text{s}^{-1}) = 10^{-3.5}$, $V(U(\text{MPa mol})) = 0$; dry olivine: $E(\text{kJ/mol}) = 154$, $n = 2.3$, $A_D(\text{MPa}^{-n} \text{s}^{-1}) = 10^{-3.5}$, $V(U(\text{MPa mol})) = 0$.

Table 2. Rheologic Parameters in the Simulations

	C_0 for the Upper Crust (MPa)	C_1 for the Upper Crust (MPa)	Magma Viscosity in the Channel (Pas)	Maximum Influx Velocity (m/yr)	FC_0 for the Upper Crust ^a
A1	50	0.8	10^{14}	270	0
A2	5	0.8	10^{14}	285	0
A3	500	0.8	10^{14}	260	0
A4	50	8	10^{14}	270	0
A5	100	3	10^{14}	270	0
A6	30	8	10^{14}	265	0
A7	2	4	10^{14}	270	0
A8	2	0.8	10^{14}	260	0
A9	10	3	10^{14}	280	0
A10	10	0.8	10^{14}	280	0
A11	10	0.3	10^{14}	280	0
A12	30	0.8	10^{14}	265	0
A13	30	0.08	10^{14}	265	0
A14	50	3	10^{14}	260	0
A15	50	0.3	10^{14}	270	0
A16	50	0.08	10^{14}	270	0
A17	100	0.8	10^{14}	270	0
A18	100	0.3	10^{14}	270	0
A19	300	8	10^{14}	255	0
A20	300	0.8	10^{14}	255	0
A21	300	0.08	10^{14}	255	0
B4	50	8	10^{15}	32	0
C4	50	8	10^{16}	7	0
D4	50	8	10^{17}	0.85	0
E1	50	0.8	10^{14}	270	0.01
E2	50	0.8	10^{14}	270	0.05
E3	50	0.8	10^{14}	270	0.1

^a $FC_1=0$ for the upper crust in all models.

$$\rho_{P,T} = \rho_0 [1 - \alpha(T - T_0)] [1 + \beta(P - P_0)] \quad (6)$$

where ρ_0 is the standard density at $P_0=0.1$ MPa and $T_0=298$ K; α and β are the thermal expansion and the compressibility coefficient, respectively.

[17] The latent heat of melting of the lower crust and crystallization of magmas is included implicitly [Gerya and Burg, 2007] by replacing C_p and α in equation (2) with, respectively, an effective heat capacity ($C_{p\text{eff}}$) and an effective thermal expansion coefficient ($\alpha_{p\text{eff}}$) of partially crystallized/molten rocks ($0 < M < 1$):

$$C_{p\text{eff}} = C_p + Q_L \left(\frac{\partial M}{\partial T} \right)_P \quad (7)$$

$$\alpha_{\text{eff}} = \alpha + \rho \frac{Q_L}{T} \left(\frac{\partial M}{\partial P} \right)_T \quad (8)$$

where C_p and α are the heat capacity and the effective thermal expansion coefficient of solid rock and Q_L denotes the latent heat of melting (Table 1).

2.3. Rheological Model

[18] To account for elastic response, viscous flow and plastic yielding the strain rate that is used in the model are defined as

$$\dot{\epsilon}_{ij} = \dot{\epsilon}_{ij(\text{viscous})} + \dot{\epsilon}_{ij(\text{elastic})} + \dot{\epsilon}_{ij(\text{plastic})} \quad (9)$$

whereby viscous, elastic, and plastic strain rate can be formulated in terms of the stress as follows:

$$\begin{aligned} \dot{\epsilon}_{ij(\text{viscous})} &= \frac{1}{2\eta} \sigma'_{ij} \\ \dot{\epsilon}_{ij(\text{elastic})} &= \frac{1}{2\mu} \frac{D\sigma'_{ij}}{Dt} \\ \dot{\epsilon}_{ij(\text{plastic})} &= X \frac{\sigma'_{ij}}{2\sigma_{II}^{1/2}}, \text{ if } \sigma_{II}^{1/2} \geq \sigma_{\text{yield}} \\ \dot{\epsilon}_{ij(\text{plastic})} &= 0, \text{ if } \sigma_{II}^{1/2} < \sigma_{\text{yield}} \end{aligned} \quad (10)$$

where η is the viscosity, μ is the shear modulus, $\sigma_{II}^{1/2}$ is the plastic potential of non-dilatant material ($\sigma_{II}=0.5\sigma_{ij}\sigma_{ji}$ is the second deviatoric stress invariant), and X is a plastic multiplier that is

satisfying the plastic yielding condition $\sigma_{II}^{1/2} = \sigma_{\text{yield}}$. σ_{yield} being the plastic yield strength of the material.

[19] The viscosity for (partially) molten rocks ($M > 0.1$) is computed as function of the melt fraction [Bittner and Schmeling, 1995] as

$$\eta = \eta_0 \exp \left[2.5 + (1 - M) \left(\frac{1 - M}{M} \right)^{0.48} \right] \quad (11)$$

where $\eta_0 = 10^{13}$ Pa s is an empirical parameter [Bittner and Schmeling, 1995]. This equation differs from the original equation proposed by Pinkerton and Stevenson [1992] and predicts similar viscosity at low melt fraction, whereas at high melt fraction, the viscosity is higher and gradually approaches $\eta_0 e^{2.5}$. This provides lower bound for the melt viscosity in our models and implies viscosity variations of $1 \cdot 10^{14} - 2 \cdot 10^{15}$ Pa s for the magma in our numerical experiments.

[20] The viscosity of magma according to this simple rheological model is higher than suggested by experimental studies [see Giordano *et al.*, 2008], which refer to crystal-free melts. The higher viscosity does not allow one to correctly resolve convection in the magma chamber. Our rheological choice is also dictated by the numerical limitations on the viscosity variations in the model ($10^{12} - 10^{26}$ Pa s). The primary focus of this study is on the intrusion emplacement rather than magma chamber convection processes [Gerya and Burg, 2007].

[21] The viscosity of solid rocks (assuming $M \leq 0.1$) depends on stress, pressure, and temperature [Ranalli, 1995]:

$$\eta = \frac{1}{2} \left(\frac{1}{\sigma_{II}} \right)^{(n-1)/2} \frac{1}{A_D} \exp \left(\frac{E + PV}{RT} \right) \quad (12)$$

where A_D (material constant), E (activation energy), V (activation volume), and n (stress exponent) are empirical flow law parameters (Table 1).

[22] Plastic deformation starts if the yield strength σ_{yield} has been reached:

$$\sigma_{\text{yield}} = C + FC \cdot P \quad (13)$$

where C is the residual strength (cohesion) at $P = 0$ and FC is the friction coefficient. In our model, we assume that brittle strength of crustal rocks in the magma emplacement area is subjected to strain-induced weakening due to the effects of percolating melts and/or magmatic fluids [e.g., Gerya and Burg, 2007; Lavier *et al.*, 2000]: C decreases linearly from C_0 to C_1 and FC decreases linearly from FC_0 to FC_1 when strain increases from γ_0 to γ_1 (Table 1).

[23] The initial yield strength of the upper crust was varied over a wide range consistent with literature values. Kohlstedt *et al.* [1995] calculated values for crustal strength of 2.5 MPa to 170 MPa under the assumption of a prefractured crust. Burov *et al.* [2003] suggested that the yield strength has values given by $0.65\rho gz \leq \sigma_y \leq 0.85\rho gz$, which leads to an upper crustal yield strength between 0.2 MPa close to the surface and 180 MPa at a depth of 10 km. In our simulations, we used values given by these intervals, from 5 MPa to 140 MPa. Values for the effective friction coefficient vary between 0.6 for $P > 200$ MPa and 0.85 for $P < 200$ MPa for dry rocks but can be significantly lower (0.01–0.1) for fluid- and melt-present crustal and mantle conditions [e.g., Gerya and Burg, 2007; Sobolev and Babeyko, 2005]. As our model is designed for regions of active melt input, we concluded that the latter case is likely applicable and used a zero friction coefficient in most of the calculations. In this case, the yield strength becomes independent of pressure and equals the cohesion. We also tested higher friction coefficients of 0.01 up to 0.1 for the upper crust (Table 2).

3. Model Description

[24] The two-dimensional model domain has a size of 1100×200 km (Figure 1) with a minimum resolution of $250 \text{ m} \times 500 \text{ m}$ in the upper central $40 \text{ km} \times 40 \text{ km}$ wide area where the intrusions develop. The large horizontal model extent was chosen to avoid boundary effects. The color coding shown in Figure 1 represents upper (grey) and lower (green) crust, lithospheric mantle (dark blue), and asthenospheric mantle (light blue) as units with different rheological properties (compare Table 1). As a generic way to represent heterogeneities within the upper crust, we included a 1 km thick layer of different crustal strength (“weak layer,” shown in dark grey in Figure 1) at a depth of 3 km. A free surface that allows the upper crust to deform vertically and to develop topography is mimicked by the “sticky air” approximation [Schmeling *et al.*, 2008], i.e., we prescribed the upper 10 km of the model to be of air-like density and significantly lower viscosity than the upper crust. The boundary conditions for velocity are free slip on all boundaries; for temperature, they are zero heat flux at the lateral boundaries, and fixed temperatures of 273 K and 1618 K on the upper and lower boundaries, respectively.

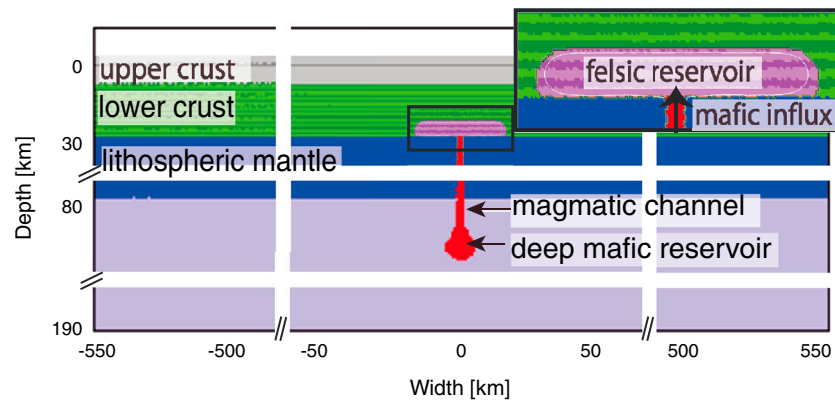


Figure 1. Model setup: The color-coding indicates different lithological units. Grey denotes the upper crust including a dark grey part identifying a weak layer within the upper crust. Green represents the lower crust; the different shading in the lower crust is employed for better visualization of deformation. The dark blue layer denotes the lithospheric, the light blue the asthenospheric mantle. The deep mafic reservoir and the magmatic channel (red) provide a continuous influx of mafic magma into the felsic reservoir (purple). Ascent of mafic melt through porous mantle is mimicked by Poiseuille flow in the channel and prescribed the viscosity within the magmatic channel. In the lower crustal hot zone, the temperature is decreasing gradually from about 1200 K at the center to about 950 K at the edges (the white line within the reservoir is the isotherm of 1073 K). For further details regarding boundary and initial conditions, see text.

[25] For the initial temperature distribution, we assumed a temperature gradient of 20 K/km within the crust (0–30 km depth), 10 K/km within the lithospheric mantle (30–100 km depth), and 0.5 K/km within the asthenospheric mantle (>100 km depth). We prescribe a positive temperature anomaly at a depth of 30 km, thought to represent a hot zone of partially molten lower crust that may have formed in response to mafic underplating and intraplate tectonics (compare, for example, *Annen et al.* [2006]). It is out of the scope of this study to model the process of how this partially molten magma originated. The initial temperature distribution in the felsic reservoir was set to be gradually decreasing from 1200 K in its center to the surrounding rock temperature. Following *Gerya and Burg* [2007], we set the reference viscosity of the magma to $\eta_0 = 10^{13}$ Pa s.

[26] Similar to *Gerya and Burg* [2007], we introduce a deep mafic reservoir that represents a thermally and chemically distinct region of partially molten rock that has a much lower viscosity than the surrounding dry mantle. Ascent of this mafic magma is commonly thought to occur through porous channels in the mantle [e.g., *Spiegelman et al.*, 2001]. As our model does not include porous flow, we approximate porous ascent by Poiseuille flow. By adjusting the viscosity within the channel we can simulate different injection rates, in this way mimicking the effect of variable permeability. The ascent is driven by the pressure difference between the deep mafic reservoir and the bottom of the upper crust as well as the buoyancy of the magma, and it is counteracted by the strength of the crust above the magmatic channel.

As soon as the mafic magma reaches the bottom of the lower crust, it is assigned a temperature-dependent viscosity. Our model setup results in continuous upflow of mafic magma (i.e., in a large single magmatic pulse) and does not account for periodic influx (i.e., for multiple smaller pulses) as has been reconstructed for natural systems.

4. Results

[27] A large number of reconnaissance simulations indicated that in the parameter space of viscoplasto-elasto rheology covered by our study, the injection of mafic mantle magma into the lower crustal felsic reservoir is crucial to initiate felsic magma ascent from a lower crustal reservoir. The buoyancy contrast between felsic magma and lower crustal host rock alone was insufficient to initiate ascent, and without mafic injection, the felsic magma just cooled and solidified at its initial position. We found that mainly three parameters influence the development of crustal felsic intrusions in response to mafic injection: (a) initial yield strength of the upper crust that defines the force to be overcome for initiating brittle/plastic failure, (b) final yield strength of the upper crust that defines the degree of strain-rate induced weakening during plastic deformation, and (c) the injection rate of mafic magma that controls the timescale of the system evolution. The influence of these parameters was then studied in detail. The model parameters for those simulations that are considered in the following are summarized in Table 2.

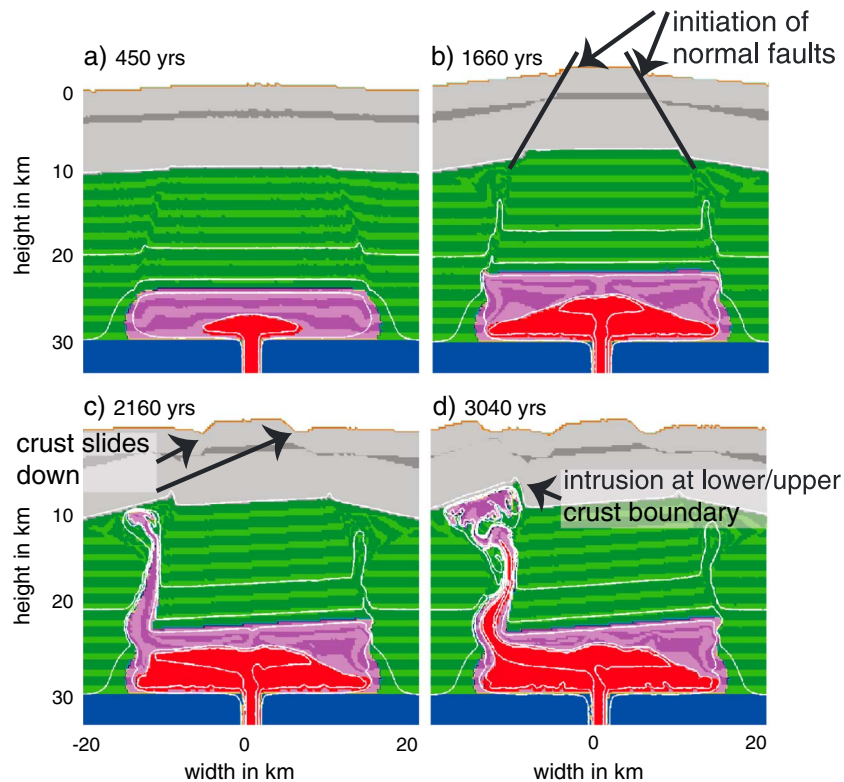


Figure 2. Temporal evolution of an exemplary simulation that shows triggering of felsic magma ascent by mafic magma intrusion into a lower crustal felsic reservoir. (a) The additional volume of the incoming mafic magma induces overpressure in the reservoir and the resulting stress field leads to the development of localized weak zones in the crust. (b) Initially, the volume increase is then compensated by surface uplift along the weak zones. (c) Magma ascends from the edges rather than the center of the reservoir and topography is compensated by extensional deformation in the uppermost crust. (d) The magma accumulates and forms an intrusion underneath the upper crust (simulation B4).

4.1. Ascent of Felsic Magma Triggered by Mafic Intrusion

[28] Figure 2 shows the general temporal evolution of calculation B4, where felsic magma ascent is triggered and leads to emplacement at upper crustal levels. Due to the pressure difference between the mafic and the felsic reservoir, mafic magma starts to rise through the magmatic channel and infiltrates the felsic reservoir (Figure 2a). In the lower crust, a strong localization of high deformation rates initiates shear zones that emerge from the upper corners of the reservoir. The volume increase is compensated by surface uplift that reaches a maximum after ca. 1660 years (Figure 2b). As high deformation rates lower the viscosity, the highly deformed regions become weaker and the magma starts to ascend within these weak zones in the lower crust; in the upper parts, extensional movements reduce the strong topography initiated by the uplift (Figure 2c). The extensional movements initiate along strongly localized zones of high deformation rates above the lateral edges of the magmatic reservoir. Here the viscosity reduction is sufficient to

initiate a downslide of the upper crust along the weak zone. Although the numerical model does not include brittle fracturing, the effect of strain-rate-induced weakening allows for the development of highly localized shear zones that develop patterns that resemble extensional faulting. When the rising felsic magma reaches the upper crust, the movement of the magma turns to horizontal direction and pluton emplacement starts. In this simulation, the intrusion forms immediately below the upper crust. A secondary uplift of the upper crust develops above the evolving intrusion. After 3040 years, the intrusive process is completed and the magma solidifies due to conductive cooling, while the shape of the intrusion is not further changing (Figure 2d).

4.2. Controls on Triggering

[29] The triggering of felsic magma ascent mainly depends on the initial yield strength of the upper crust. Figure 3 shows three end-member cases where only the initial yield strength of the upper crust was varied (5 MPa, first row; 50 MPa, second row; and 500 MPa, third row); all other parameters

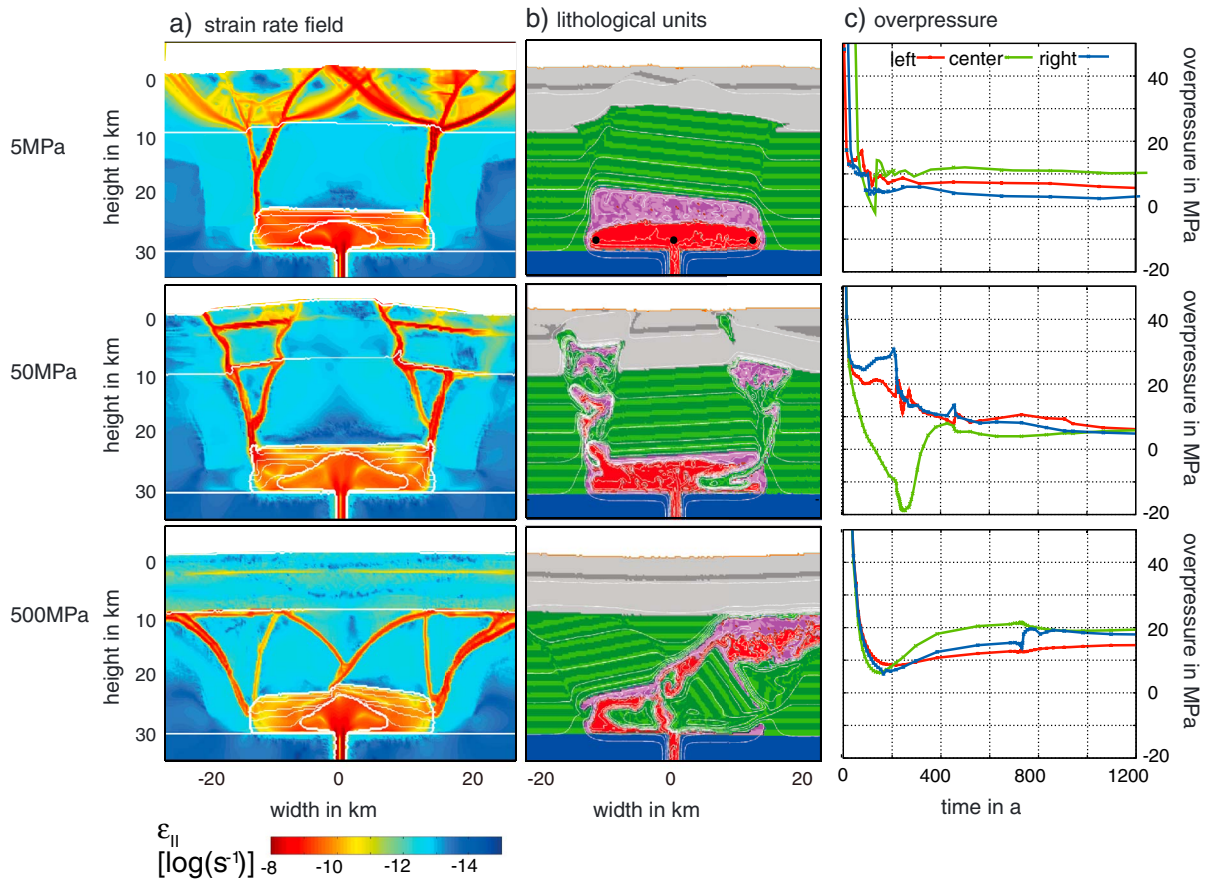


Figure 3. Influence of initial yield strength on triggering ascent and intrusion. Rows show different initial yield strengths: 5 MPa, calculation A2 (first row); 50 MPa, calculation A1 (second row); and 500 MPa, calculation A3 (third row). Columns show (a) strain-rate distribution at the moment of highest topography, (b) lithological units in the final state of the simulation, and (c) temporal evolution of overpressure (computed at the locations of the three black dots indicated in Figure 3b in the first row).

were kept constant. In each row, we show (a) the second invariant of the strain-rate tensor (a measure for the rate of deformation) at the moment of highest topography, (b) the lithological units, and (c) the temporal evolution of overpressure, defined as total pressure minus lithostatic load at a given point. The overpressure is measured at three different locations within the lower crustal reservoir that are marked in the illustration of the lithological units. Positive or negative overpressure indicates the difference between the lithostatic load and the isotropic pressure distribution in the (partially) molten reservoir. Depending on the initial yield strength, the localization of deformation and the mechanism of space generation are different.

[30] The first row of Figure 3 shows the system development in the case of a weak upper crust (initial yield strength of 5 MPa). The strain-rate field shows a strong localization of the shear zones in the lower crust that are nearly vertical and

emerge from the upper corners of the felsic reservoir. Within the upper crust, shear zones are more abundant and nucleate where lower crustal shear zones reach the upper crust. The stress pattern within the upper crust is not affected by the weak layer because the contrast in strength is insufficient. The upper crust escapes sideward along shear zones and only slight topography develops. Hence, space for the additional volume of the incoming mafic magma is generated by thinning of the upper crust. In the temporal evolution of overpressure in the felsic reservoir, there are no significant differences between the center and the lateral edges. Ascent of felsic material from the reservoir is not triggered.

[31] The second row of Figure 3 shows a case of a stronger crust with an initial yield strength of 50 MPa. The regions of high deformation rates are strongly localized both within the lower crust and the upper crust. The upper crustal weak layer accommodates high deformation rates. Space is

generated by strong uplift of the upper crust. This uplift causes a horizontal variation of the lithostatic load within the felsic reservoir. The location of the maximum lithostatic load correlates with the highest elevation above the center of the reservoir. The magma within the felsic reservoir behaves like an isotropic fluid, i.e., the total pressure is constant at a certain depth level within the reservoir. Therefore, the overpressure varies horizontally within the reservoir, being negative at the center of the reservoir (Figure 3c, second row) while a strong overpressure develops at the lateral edges and forces the felsic magma to ascent from there. In the visualization of the lithological units, the evolving plutons are located at different depths in the upper crust. Both plutons developed at a transition from weaker to stronger material. The top of the left pluton is located at the depth of the weak layer while the top of the right one is underlying the upper crust.

[32] The third row of Figure 3 depicts the development of the system for a very strong upper crust (initial yield strength of 500 MPa). The deformation is highly localized within the lower crust. Shear zones form not only from the lateral edges of the felsic reservoir but also from the center. In the upper crust only, the weak layer displays elevated deformation rates. The remainder of the upper crust does not develop weak zones as the strength is sufficient to resist deformation. The differential uplift of crustal material is only marginal; therefore, the overpressure shows no significant differences between the center and the lateral edges. Space for the incoming mafic magma is neither generated by a significant vertical surface uplift, nor by thinning of the upper crust. Rather, space is generated by a combination of viscous flow of the lower crust along the weak zones in horizontal direction away from the felsic reservoir and a minimal surface uplift over a wide area. No discrete triggering and ascent of felsic magma from the reservoir is observed. However, the magma eventually becomes mobilized because strong movement of a large block of lower crustal material along weak zones forces it to escape and to pool below the upper crust, leading to the formation of a large pluton. The illustration of the lithological units reveals (Figure 3b, third row) that the topography of the final shape of the system is lowest in the center and more elevated at distances of >20 km from the center.

4.3. Controls on Intrusion Style

[33] While the initial yield strength of the upper crust controls whether ascent of felsic magma is

triggered, the combination of initial and final yield strength influences the style of intrusion, namely the level of emplacement and the shape of the intrusion. For an intermediately strong crust where ascent of felsic magma is triggered (see Figure 3b), we find four different styles of intrusions that are shown in Figure 4. For all cases, the ascent of felsic magma is triggered by the overpressure differences between the center and the lateral edges of the felsic reservoir.

[34] Upon increasing initial strength above values for the end-member case of a very weak crust (Figure 3a), vertical ascent of felsic magma from one of the upper corners of the reservoir is initiated but comes to a halt within the lower crust (Figure 4a). Further increase of the initial yield strength allows the development of higher overpressure differences in the reservoir and leads to magma ascent into upper crustal levels and the formation of intrusions (Figure 4b). For further increased initial yield strength, we found the upper crust to be too strong to develop weak zones and the ascending magma is accumulating as sills underneath the upper crust but does not intrude it (Figure 4d). An even stronger crust prohibits triggering of magma ascent, as the crust is not bending enough that sufficient overpressure differences can develop within the felsic reservoir (Figure 3c, end-member case).

[35] The final yield strength does not generally change these cases but moderately modulates the exact values of the initial yield strength at which the transition between these intrusion styles happen (Figure 4, diagram). Furthermore, for an initial yield strength between 20 and 80 MPa and low final yield strength, we found magma completely breaking through the upper crust (Figure 4c). In this parameter range, the rheological contrast between the weak layer and the rest of the upper crust is insufficient to stop the magma ascent at the depth of the weak layer. However, final yield strengths above approximately 2 MPa appear to inhibit such breakthrough.

4.4. Controls on Timescales

[36] In cases with an intermediately strong crust and triggering of felsic magma ascent, the timescale of the early system evolution is governed by the injection rate of mafic magma into the felsic reservoir. The overall geometry of evolving structures in the system (zones of high deformation rates, surface uplift, and the triggering of felsic magma ascent itself) is essentially independent

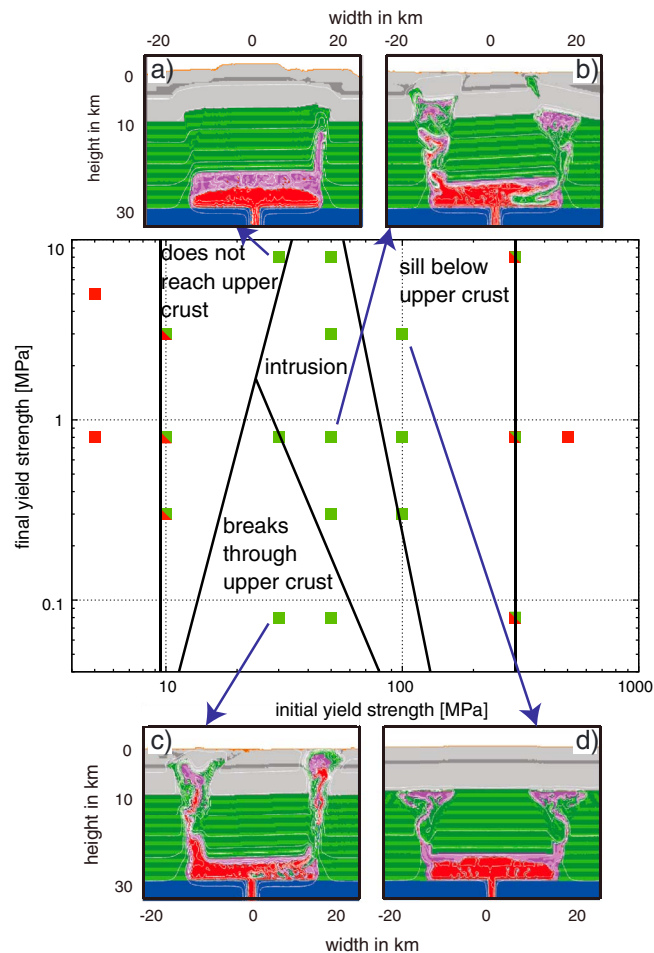


Figure 4. Intrusion styles as a function of initial and final yield strength. The red squares in the central diagram indicate simulations in which no triggering from the edges of the reservoir was observed. The green squares indicate conditions where triggering was observed; these conditions are subdivided according to different final intrusion shapes and levels were attained as illustrated by Figures 4a–4d. For further detail, see text. The initial and final yield strengths for the examples are (a) $\sigma_I=30$ MPa, $\sigma_F=8$ MPa, calculation A6; (b) $\sigma_I=50$ MPa, $\sigma_F=0.8$ MPa, calculation A1; (c) $\sigma_I=30$ MPa, $\sigma_F=0.08$ MPa, calculation A13; and (d) $\sigma_I=100$ MPa, $\sigma_F=3$ MPa, calculation A5.

of the injection rate, but the time required to develop the structures correlates with injection rates. Figure 5 illustrates the temporal evolution of overpressure, determined in the center and at the right edge of the reservoir, for three different viscosities (and hence influx rates) of the ascending mafic magma within the channel. All other parameters are kept constant (Table 3). The black vertical lines indicate the instant where felsic magma starts to ascend from the reservoir in the different calculations. The magma ascent from the lateral edges coincides with a sudden decrease of overpressure at these edges of the magma chamber. For each influx rate, the field of the deformation rate is shown on the right-hand side in Figure 5. The upper diagram shows the field for the fastest and the lowermost one for the slowest influx rate, respectively.

[37] For all influx rates, a sufficient difference in overpressure between the center and the lateral edges of the felsic reservoir develops. The time required to evolve this overpressure difference is strongly dependent on the injection rate. While the maximum overpressure difference is reached after about 170 years for the lowest channel viscosity (10^{14} Pa s, fastest influx velocity) it lasts about 11,000 years until it is reached for the largest channel viscosity (10^{16} Pa s, slowest influx rates).

[38] A lower injection rate causes lower rates of deformation in the system, and therefore, the decrease of viscosity in the weak zones is minor. For all injection rates displayed in Figure 5, weakening is sufficient for the generation of weak zones, thus allowing magma ascent. However, at even slower injection rates (viscosity within the channel

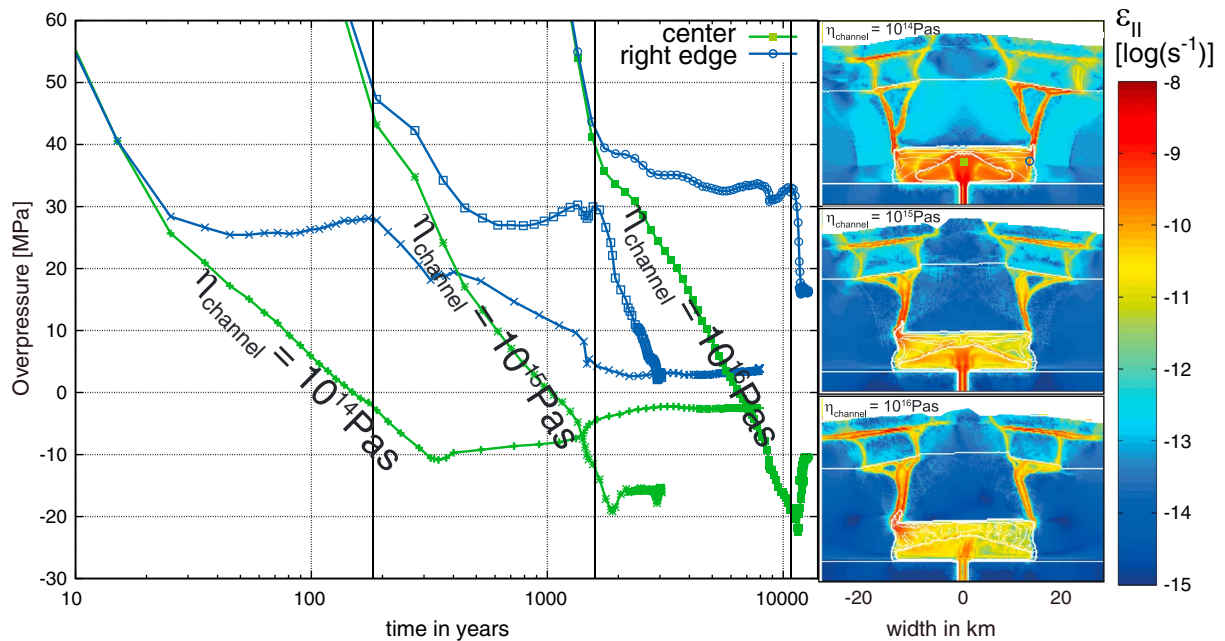


Figure 5. Temporal evolution of overpressure for three different channel viscosities. The overpressure is measured at the center (green) and the right edge (blue) of the reservoir (compare Figure 3), and the field of the deformation rate for each injection rate is shown at the time of the minimum overpressure at the center of the reservoir. The injection rate is governing the time scale of the system while the qualitative behavior of the system is the same. The black lines mark the beginning of magma ascent from the edges of the felsic reservoir (calculation A4 with a channel viscosity of 10^{14} and an injection rate of 270 m/a, calculation B4 with a channel viscosity of 10^{15} and an injection rate of 32m/a, and calculation C4 with a channel viscosity of 10^{16} and an injection rate of 7m/a).

10^{17} , injection rate about 1 m/yr), felsic magma ascent was not triggered.

4.5. Sensitivity to Friction Coefficient

[39] As the strength of the upper crust is dependent not only on the cohesion but also on the friction coefficient, we performed some simulations with nonzero friction coefficient FC_0 for the upper crust that are shown in Figure 6. The result for a friction coefficient of 0.01 (Figure 6b) is similar to the result of a zero friction coefficient (Figure 6a). The upper crustal intrusions are slightly smaller but in the same places. With increasing friction coefficient, the intrusion patterns start to resemble those of crust with stronger cohesion but a zero friction coefficient (Figures 6c and 6d; compare Figure 3).

5. Discussion

5.1. Felsic Magma Ascent Driven by Mafic Mantle Magma Injection

[40] Our simulations show that injection of mafic mantle magma into a lower crustal felsic magma reservoir induces overpressure that can trigger felsic magma ascent. Key factors that control the ascent are crustal failure and differential uplift that develop in response to overpressure, and both strongly depend on crustal rheology. In the parameter space of visco-plasto-elasto rheology covered by our study, the buoyancy contrast between felsic magma and lower crustal host rock alone was insufficient to initiate felsic magma ascent from the reservoir.

Table 3. Averaged Uplift Rates, Ascent and Intrusion Times for Different Influx Velocities

	C_0 for the Upper Crust (MPa)	C_1 for the Upper Crust (MPa)	Magma Viscosity in the Channel (Pas)	Time Before Ascent (years)	Average Uplift Rate (cm/yr)	Ascent Duration (years)	Time of Intrusion (years)
A4	50	8	10^{14}	174	1100.5	144	927
B4	50	8	10^{15}	1563	100.3	485	1052
C4	50	8	10^{16}	11057	18	1134	1350

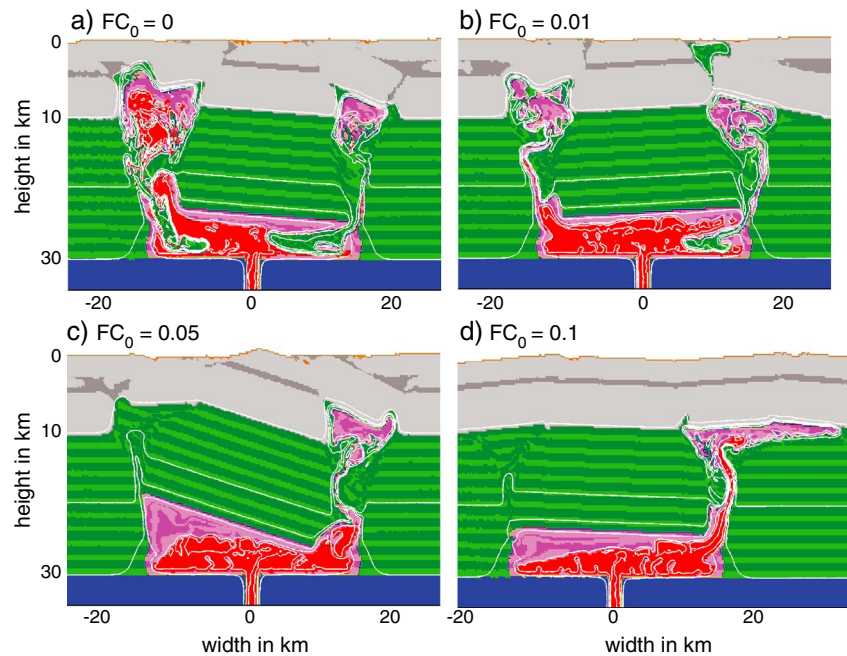


Figure 6. Simulations with different initial friction coefficients (FC_0) of the upper crust after a time of about 2300 years (simulations A1, E1, E2, and E3 from Table 2). The main effect of an increasing initial friction coefficient is a higher initial yield strength of the upper crust; the resulting intrusion styles develop in a fashion similar to the effect of increasing cohesion at zero friction coefficient (compare the middle and bottom panels of Figure 3b).

[41] Magma ascent typically initiates from the lateral edges of the felsic reservoir as weakest zones within the lower crust develop between the lateral edges of the felsic reservoir and the bottom of the lower crust. The localization of the weak zones reflects that the highest stresses in the host rock develop close to the upper lateral edges of the overpressured magma chamber where the highest curvature of the magma-host rock interface is located [Gudmundsson, 2006]. As we allow for surface uplift, the geometrical causes studied by Gudmundsson [2006] will compete with the effects of surface uplift, thinning of the upper crust, and/or horizontal movements within the lower crust (Figure 3) in determining the stress and deformation rate distribution. Sufficient overpressure to drive magma ascent develops for intermediate and high upper crustal strengths. A weak upper crust dissipates overpressure and stresses induced by the inflation of the lower crustal reservoir and no ascent is triggered.

[42] The most efficient and dynamic ascent mechanisms develop for intermediate upper crustal strengths. For these, a strong topography with highest elevation above the center of the reservoir can develop. The difference in lithostatic load induces a heterogeneous horizontal overpressure distribution in the reservoir as the magma responds like an isotropic fluid. The lateral edges experience significant

overpressure while the center of the reservoir is underpressured (Figures 3c, middle row, and 5). This provides a strong driving force for felsic magma escape from the lateral edges of the reservoir, which is further favored by the development of weak zones in the same locations. Hence, the development of topography is a major control in this process. It seems likely that preexisting topography (e.g., volcanic edifices in arc settings) may notably facilitate the ascent of felsic magma and may play a major role in determining the position of felsic magma intrusion. An intermediate crustal strength in our model is also required for felsic magma ascent into upper crustal levels.

[43] Strong upper crustal rheology allows sufficient overpressure to develop for triggering magma ascent. However, it prevents the magma from intruding the upper crust and large intrusions form at the lower-upper crust boundary. A strong upper crust may therefore be essential for the formation of mid-crustal batholiths.

5.2. Intrusion Shapes and Controls on Emplacement

[44] Once triggered, the felsic magma ascends within the crust and finally arrests at a certain depth. In our model, this is mostly dependent on the upper crustal strength.

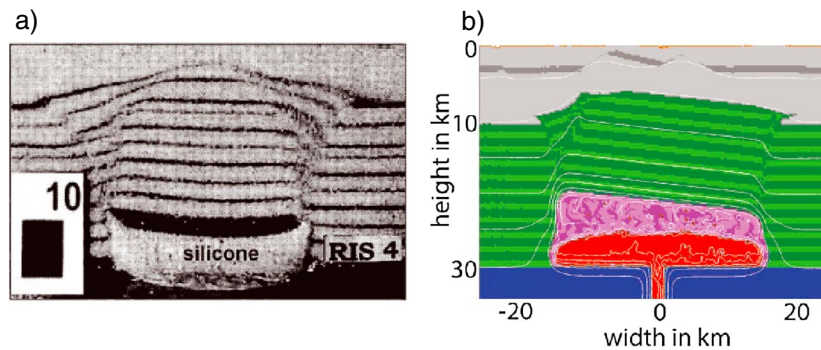


Figure 7. Comparison of a calculation with (left) our model with a (right) visualization of analogue models of pluton emplacement [Acocella and Mulugeta, 2001]. A model with rather weak upper crust has been selected inferring a small difference in strength between upper and lower crust (simulation A2).

[45] For a weak upper crust, our model predicts the formation of large, composite lower crustal magma bodies, generated by the inflation in response to mafic magma injection. The lower crustal bodies and associated deformation structures that develop in our model are similar to those of analogue sand-box models with injected silicone [Acocella and Mulugeta, 2001]. Figure 7a shows an example of silicone intruding into a layer of sand, causing uplift of the intrusion and the development of localized deformation zones that emerge from the upper lateral edges. These closely resemble the geometries that develop in our models (Figure 7b) with a weak upper crust.

[46] Many of our simulations with intermediate or strong upper crustal rheology display the arrest of magma ascent with a concomitant horizontal spreading of the intrusion. We observed that the tops of the intrusions are located at rigidity boundaries, namely the transition from lower to upper crust and the weak layer within the upper crust (compare Figure 4). In analogue experiments, Kavanagh *et al.* [2006] demonstrated that sill formation in a homogeneous crust is impossible without extensional or compressive pressures. Without allowing for an external stress field, rigidity contrasts were required to force sill intrusions by stopping magma ascent. Menand *et al.* [2011] point out that rigid layers can favor sill formation due to arresting the vertical propagation of a feeder dyke. Field examples for the deflection of dykes into sills at discontinuities were given by Gudmundsson [2011]. He provided a numerical model with a detailed analysis of the stress field generated from a propagating dyke in the presence of layers of different stiffness. If the upper layer is stiffer than the lower layer, a sill forms likely within the lower layer, which agrees with our observation that most sill-like intrusion form below stronger material, e.g.,

at the lower-upper crust boundary in models with a strong upper crust.

[47] Besides the formation of intrusions, we observed in some numerical models that the magma stopped during ascent within the homogeneous lower crust without any horizontal movement. In this case (Figure 4a), no rheological contrast was responsible for the arrest of magma ascent. Menand [2011] explains that dike arrest at a level of neutral buoyancy is likely for dikes but not for sill formation. In our model, the dike-like structure did not stopped at the level of neutral buoyancy, nor could its arrest be explained by neutral buoyancy, as the ascent is caused by an additional overpressure due to the surface topography that develops in the calculations. Rather, the dike arrest occurs because the driving forces (buoyancy and the differences in overpressure) are neutralized by the restoring force, which is the resistance of the crustal material.

5.3. Timescales

[48] In order to evaluate the timescales predicted by our models, we divide the evolution of the system into different stages that are comparable with field or modeling data from the literature. These are (1) the injection of the mafic magma into the lower crustal felsic reservoir, which is not an outcome of the model but an input parameter; (2) the initial surface uplift from the ascent of mafic injections until the moment where the crust fails (which correlates well with the time at which the ascent of felsic magma starts); and (3) the subsequent, self-consistent evolution of ascent and emplacement.

5.3.1. Injection Rate

[49] In natural systems, the ascent of mafic magma within the mantle is proposed to proceed via porous

flow. As the simulation code does not include porous flow, we prescribed the ascent of mafic magma as viscous flow in a magmatic channel. The influx rate was controlled by defining the viscosity of the mafic material within the magmatic channel. The ascent velocity can then be calculated via a channel flow equation and is proportional to the inverse of the magma viscosity within the channel ($v \sim \eta^{-1}$). The ascent rates in the model range from 0.85 m/yr to 280 m/yr (Table 2). *Turner and Costa* [2007] estimated similar and even higher magma ascent velocities moving through mantle wedges. They assume high porosity channels where the magma reaches velocities of 10–1000 m/yr. As long-term crustal addition rates in subduction-related arcs are much slower (on the order of 20 km²/Myr [*Vogt et al.*, 2012]), such high rates would probably imply short underplating pulses separated by longer periods of inactivity.

5.3.2. Uplift of the Upper Crust

[50] Significant uplift of the crust occurs for crust of intermediate strength until the felsic magma starts to escape from the reservoir (Table 3). Therefore, its duration is strongly dependent on the injection rate of mafic magma. In case of fast mafic injection (channel viscosity of 10¹⁴ Pas; maximum injection velocity 270 m/a) the average uplift velocity of 11.5 m/a is exceptionally high and geologically unrealistic. The uplift velocity of 18 cm/a in the case of a slow injection rate (channel viscosity of 10¹⁶ Pas; maximum injection velocity 7 m/a), however, approaches actual field data. Crustal uplift in natural systems reveals an uplift velocity up to 2.2 cm/a in the Yellowstone caldera [*Dzurisin et al.*, 1994], or year-to-year elevation changes up to 3–4 cm for the inflation of the Three Sisters volcanic center [*Riddick and Schmidt*, 2011]. At Iwo-Jima, the emergent part of a large submarine volcano in the western Pacific, a long-term uplift rate of 15–20 cm/a was estimated over the last centuries. The uplift is probably caused by magma intruding into a sub-caldera reservoir [*Kaizuka*, 1992]. In these examples, the uplift lasts over a timescale of tens to hundreds of years and has been attributed to intrusions in upper crustal levels (5–7 km depth). Our models predict that similar uplift rates may also be induced by lower crustal magmatism. Geophysical evidence such as intrusion-related seismicity would probably be required to distinguish between the two possibilities in natural examples.

[51] There is also evidence for surface uplift caused by magmatic underplating or intrusion into the deep lower crust: *Cox* [1993] underlines that continental

magmatic underplating caused surface uplift of at least 1 km in the area of the Karoo province. Uplift of Scotland, caused by magmatic underplating, was reconstructed by regional sea level changes. Here magmatic material was added to the lithosphere at a depth of about 30 km beneath western Scotland over a period of 60 Ma [*MacLennan and Lovell*, 2002]. The possible uplift by magmatic underplating can thus be calculated by $h_{\text{uplift}} = h_{\text{melt}}(\rho_{\text{melt}} - \rho_{\text{crust}}) / \rho_{\text{melt}}$ and results for $\rho_{\text{melt}} = 2600 \text{ kg/m}^3$ and $\rho_{\text{crust}} = 3000 \text{ kg/m}^3$ a maximum uplift of 1.2 km for a melt layer of 8 km thickness. An even higher uplift of about 2.5 km related to magmatic intrusions is proposed based on reconstruction for the Amiata area in southern Tuscany [*Acocella*, 2000].

5.3.3. Felsic Ascent

[52] The duration of ascent and emplacement is summarized in Table 3 for different channel viscosities. Initial and final yield strengths are kept constant. Following *Petford et al.* [2000], we define the transition between ascent and emplacement as the transition from vertical to horizontal movement (Figure 2, time evolution). The duration of ascent and emplacement of magma displays little dependence on the injection rate. Ascent of felsic magma prior to emplacement lasts about 140 to 1100 years; the time for the emplacement process is in the range of about 900 to 1300 years (Table 3) while material is still ascending and thus feeding the evolving intrusion during emplacement. The injection rate influences mainly the timescale on which the lower crustal felsic reservoir is inflated but not the timescale of the intrusion processes itself.

[53] From field-based studies, much longer timescales have been inferred for the formation of large felsic plutons. For example, *Michel et al.* [2008] suggest an incremental growth of the Torres del Paine laccolith in Patagonia over 90 kyr. We did not consider incremental growth by multiple batches of magma; rather, our model represents the scenario of a single batch. The emplacement of a single batch in such a periodically growing system happens on much shorter time scales and is likely in the range of the timescales resulting from our model. The Torres del Paine granites show brittle contacts between the pulses, which is a hint that the time elapsed between two pulses was long enough for significant cooling [*Leuthold et al.*, 2012]. *Michel et al.* [2008] argued that the emplacement time of the batholith of 90 kyr provides enough time for conductive cooling between two pulses as thermal diffusion would

advance $h = 1700$ m within a time $t = 90$ kyr (assuming a thermal diffusivity of $\kappa = 10^{-6}$ m²/s; $t = h^2/\kappa$), while single intrusive layers have a maximum thickness of 800 m and would require 20 kyr for solidifying. *de Saint Blanquat et al.* [2011] pointed out that the time required for batholith formation is strongly dependent on the size of the pluton and the emplacement can vary between magmatic episodes and single magmatic pulses. Most of the magma chambers developing in our models have a horizontal extent of 5 km (x direction) and a vertical extent of 2 km (z direction). Assuming the extent of the horizontal direction to be equal in both directions (x and y), we obtain an emplaced volume of 50 km³. This is a size that is similar to a single batch of granitic magma in the Torres del Paine laccolith (Granite III in *Leuthold et al.* [2012]). *De Saint Blanquat et al.* [2011] compiled data from several field areas to estimate the relationship between volume of magmatic batches and the duration of their intrusion. For an intrusion of a magma batch of about 50 km³, they found durations of about 100 years for fast construction rates (Elba island) and up to 50 kyr to 500 kyr for slow construction rates (Emerald lake; Tinos). *Petford et al.* [2000] compared ascent and emplacement duration from different field studies that estimated timescales. They concluded that ascent lasts 0.1–100 years for the case of deformation-assisted flow and emplacement lasts 100–10,000 years. The timescales that we found in our models for the duration of ascent and emplacement match well with the range of *Petford et al.* [2000] (compare Table 3).

5.4. Model Limitations

[54] While the above discussion demonstrates that a number of results from our models are in good agreement with natural observations and independent modeling studies, we would like to emphasize that they are subject to numerical limitations and simplifications employed to translate the physical complexity of the magma emplacement processes, which is rather difficult to model, in to a numerically treatable model [e.g., *Christiansen, 2005; Dufek and Bergantz, 2005; Dufek and Bachmann, 2010; Gerya and Burg, 2007; Petford, 1996; Petford et al., 2000* and references therein].

[55] The simple magma viscosity model (equation (11)) adopted in our calculations is independent of melt composition. According to this model [*Bittner and Schmeling, 1995*], pure melt viscosity is assumed to be constant and independent of pressure, temperature, and water content. For such end-member rheology of crystal-free silicic melts, comprehensive

viscosity models are available. *Giordano et al.* [2008] developed a viscosity model with non-Arrhenian temperature dependence that covers a wide range of magma compositions, including the effect of dissolved H₂O. Pressure variations were not included in their model. The experimental results of *Ardia et al.* [2008] indicate that the viscosity of felsic melts will slightly decrease from ambient pressure to lower crustal conditions. In the limit of pure melt, the viscosity employed in our simulation would be orders of magnitudes larger than that predicted by these models. This high pure melt viscosity used in our simulations is also a result of numerical limitations for the viscosity contrast. However, pure melt conditions are unlikely to apply to the deep, felsic reservoir on the continuum scale of our calculations. The reservoir is considered a partially molten region of the lower crust, and hence, the viscosity of a mixture of melt and residual (suspended) solids is required. *Costa et al.* [2009] provided a parameter study of the influence of crystals on magma viscosities. They calculate an increase of viscosity close to the critical solid fraction up to 8 orders of magnitude, which would broadly correspond to the viscosities used in our study. In our model, even such high-viscosity materials can be mobilized, which may indicate that perfect segregation of melt from the source region is not required for the initial phases of felsic magma ascent. Due to the lack of reliable geological field constraints, the actual viscosities at depth cannot be inferred and this conclusion can, therefore, currently not be verified.

[56] The considerably lower magma viscosities at low crystal fraction may possibly be more important along the ascent path where melt segregation might be more complete and upon intrusion of the magma in shallower crustal levels. For the latter, they would be important to resolve magma chamber dynamics such as internal convection, magma mixing, and cooling dynamics as well as sudden magma degassing or crystal lockup that will change the viscosity by orders of magnitude over a rather small P - T range [e.g., *Christiansen, 2005; Dufek and Bergantz, 2005; Dufek and Bachmann, 2010; Jellinek et al., 1999; Ruprecht et al., 2012; Sparks and Marshall, 1986*].

[57] The mafic magma addition to the crust was modeled as a single pulse, whereas multiple magmatic activity episodes are often found for batholithic intrusions in nature. Likely, the integration of the model presented here into larger-scale thermomechanical simulations of magma generation in various tectonic settings might resolve how the various timescales may be linked in cases of lower mafic magma emplacement rates and/or periodic mafic magma supply. Finally, the compressibility

of magma and gas/liquid/solid fractionation is neglected in our model, which can strongly affect melt pressure and volume variations during and after the emplacement [e.g., Tarasewicz *et al.*, 2012].

6. Conclusions

[58] Our numerical simulations demonstrate that injection of mafic magma from a mantle source into a lower crustal felsic magma reservoir is a viable mechanism to trigger the ascent of felsic magma and its intrusion in upper crustal levels. Hence, mafic underplating and mafic intrusion into lower crustal reservoirs, which are thought to be an important process for generation of felsic magmas in a wide range of tectonic settings, may equally be important for initiating and controlling the transfer of felsic magma to upper crustal levels.

[59] The first-order physical effect of mafic injection is the development of overpressure within the felsic reservoir, which induces crustal failure and surface uplift. Failure and uplift are crucial for ascent of felsic magma by creating pathways and a driving force and are mainly governed by the upper crustal strength. A particularly efficient mechanism operates at intermediate upper crustal strengths, for which high topography develops above the center of the reservoir. As the melt in the reservoir acts as an isotropic fluid, underpressure develops in the reservoir center and pronounced overpressure near its lateral edges, which triggers felsic magma ascent. This may imply that preexisting strong topography—e.g., in volcanic arcs—could be an additional control, increasing the favorability of felsic magma ascent and intrusion into the upper crust.

[60] Within the studied range of rheological parameters, the height of surface uplift is mostly dependent on the initial yield strength of the upper crust; therefore, the initial yield strength is the principal rheological control on triggering of felsic magma ascent. In addition, the upper crustal strength controls the level to which the felsic magma may ascend. For an intermediately strong crust, intrusion of magma into upper crustal levels is possible, while for a weak crust, intrusions remain in the lower crust and no magma ascent is triggered. For a strong upper crust, felsic magma ascent is triggered but intrusions form only at the boundary between the lower and upper crust. The intrusion depth may further be modulated by the final yield strength, which is the major control on the shape of the developing intrusion.

[61] The injection rate of mafic magma into the felsic reservoir mainly affects the timescale of the early overpressure growth stage and the resulting rate of surface uplift. The actual ascent velocities of felsic magma and the times required for the intrusion process appear to be largely independent of the mafic injection rate. Predicted rates of surface uplift induced by the deep mafic intrusion can resemble those that have so far attributed to mid-crustal or upper crustal intrusions. If these predictions are correct, the combination of direct measurement of surface uplift with geophysical methods may be a possible route to better constraining the rates and magnitudes of mafic underplating in nature.

Acknowledgment

[62] We gratefully acknowledge the detailed, constructive, and insightful comments by two anonymous reviewers and associate editor Thorsten Becker, which helped greatly in sharpening our ideas and improving the manuscript. This research was supported by the Swiss National Science Foundation, grant 200021_125307.

References

- Acocella, V. (2000), Space accommodation by roof lifting during pluton emplacement at Amiata (Italy), *Terra Nova*, *12*(4), 149–155, doi:10.1046/j.1365-3121.2000.00286.x.
- Acocella, V., and G. Mulugeta (2001), Surface deformation induced by pluton emplacement: The case of Amiata (Italy), *Phys. and Chem. Earth Part A—Solid Earth Geodesy*, *26* (4–5), 355–362, doi:10.1016/S1464-1895(01)00065-5.
- Annen, C., and R. S. J. Sparks (2002), Effects of repetitive emplacement of basaltic intrusions on thermal evolution and melt generation in the crust, *Earth Planet. Sci. Lett.*, *203*(3–4), 937–955, doi:10.1016/S0012-821X(02)00929-9.
- Annen, C., J. D., Blundy, and R. S. J., Sparks (2006), The genesis of intermediate and silicic magmas in deep crustal hot zones, *J. Petrol.*, *47*, 505–539.
- Annen, C. (2011), Implications of incremental emplacement of magma bodies for magma differentiation, thermal aureole dimensions and plutonism-volcanism relationships, *Tectonophysics*, *500*, 3–10, doi:10.1016/j.tecto.2009.04.010.
- Ardia, P., D. Giordano, and M. W. Schmidt (2008), A model for the viscosity of rhyolite as a function of H₂O-content and pressure: A calibration based on centrifuge piston cylinder experiments, *Geochim. Cosmochim. Acta*, *72*, 6103–6123, doi:10.1016/j.gca.2008.08.025.
- Atherton, M. P. (1993), Granite magmatism, *J. Geol. Soc.*, *150*, 1009–1023, doi:10.1144/gsjgs.150.6.1009.
- Bergantz, G. W. (1989), Underplating and partial melting—Implications for melt generation and extraction, *Science*, *245*(4922), 1093–1095, doi:10.1126/science.245.4922.1093.
- Bittner, D., and H. Schmeling (1995), Numerical modeling of melting processes and induced diapirism in the lower crust, *Geophys. J. Int.*, *123*(1), 59–70, doi:10.1111/j.1365-246X.1995.tb06661.x.

- Bons, P. D., J. Arnold, M. A. Elburg, J. Kalda, A. Soesoo, and B. P. van Milligen (2004), Melt extraction and accumulation from partially molten rocks, *Lithos*, *78*, 25–42, doi:10.1016/j.lithos.2004.04.041.
- Brown, M. (2007), Crustal melting and melt extraction, ascent and emplacement in orogens: Mechanisms and consequences, *J. Geol. Soc.*, *164*, 709–730, doi:10.1144/0016-76492006-171.
- Buiter, S. J. H., A. Y. Babeyko, S. Ellis, T. V. Gerya, B. J. P. Kaus, A. Kellner, G. Schreurs, and Y. Yamada (2006), The numerical sandbox: Comparison of model results for a shortening and an extension experiment, in *Analogue and Numerical Modelling of Crustal-Scale Processes*, edited by S. J. H. Buiter, and G. Schreurs, Geological Society (London) Special Publication, pp. 29–64, doi:10.1144/GSL.SP.2006.253.01.02.
- Burg, J. P., J. L. Bodinier, T. Gerya, R. M. Bedini, F. Boudier, J. M. Dautria, V. Prikhodko, A. Efimov, E. Pupier, and J. L. Balanec (2009), Translithospheric mantle diapirism: Geological evidence and numerical modelling of the Kondyor zoned ultramafic complex (Russian Far-East), *J. Petrol.*, *50*, 289–321, doi:10.1093/petrology/egn083.
- Burov, E., C. Jaupart, and L. Guillou-Frottier (2003), Ascent and emplacement of buoyant magma bodies in brittle-ductile upper crust, *J. Geophys. Res.*, *108*(B4), 2177, doi:10.1029/2002JB001904.
- Christiansen, E. H. (2005), Contrasting processes in silicic magma chambers: Evidence from very large volume ignimbrites, *Geol. Mag.*, *142*, 669–681, doi:10.1017/S001675680500144.
- Clauser, C. H., E. Huenges (1995), Thermal conductivity of rocks and minerals, in *Rock Physics and Phase Relations*, edited by T. K. Ajrems, pp. 105–126, American Geophysical Union, Washington, D. C.
- Costa, A., L. Caricchi, and N. Bagdassarov (2009), A model for the rheology of particle-bearing suspensions and partially molten rocks, *Geochem. Geophys. Geosyst.*, *10*, Q03010, doi:10.1029/2008GC002138.
- Cox, K. G. (1993), Continental magmatic underplating, *Philos. Trans. R. Soc. London, Ser. A-Math, Phys, Engineer. Sci.*, *342*(1663), 155–166.
- De Saint Blanquat, M., E. Horsman, G. Habert, S. Morgan, O. Vanderhaeghe, R. Law, and B. Tikoff (2011), Multiscale magmatic cyclicality, duration of pluton construction, and the paradoxical relationship between tectonism and plutonism in continental arcs, *Tectonophysics*, *500*, 20–33, doi:10.1016/j.tecto.2009.12.009.
- Ducea, M. N., and J. B. Saleeby (1998), The Age and origin of a thick mafic-ultramafic keel from beneath the Sierra Nevada batholith, *Contrib. Mineral. Petrol.*, *133*(1–2), 169–185, doi:10.1007/s004100050445.
- Dufek, J., and G. W. Bergantz (2005), Lower crustal magma genesis and preservation: A stochastic framework for the evaluation of basalt-crust interaction, *J. Petrol.*, *46*, 2167–2195, doi:10.1093/petrology/egi049.
- Dufek, J., and O. Bachmann (2010), Quantum magmatism: Magmatic compositional gaps generated by melt-crystal dynamics, *Geology*, *38*, 687–690, doi:10.1130/G30831.1.
- Dzurisin, D., K. M. Yamashita, and J. W. Kleinman (1994), Mechanisms of crustal uplift and subsidence at the Yellowstone caldera, Wyoming, *Bull. Volcanol.*, *56*(4), 261–270, doi:10.1007/BF00302079.
- Gerya, T. V., and D. A. Yuen (2003), Characteristics-based marker-in-cell method with conservative finite-differences schemes for modeling geological flows with strongly variable transport properties, *Phys. Earth Planet. Inter.*, *140*(4), 293–318, doi:10.1016/j.pepi.2003.09.006.
- Gerya, T. V., and J.-P. Burg (2007), Intrusion of ultramafic magmatic bodies into the continental crust: Numerical simulation, *Phys. Earth Planet. Inter.*, *160*, 124–142, doi:10.1016/j.pepi.2006.10.004.
- Gerya, T. V., and D. A. Yuen (2007), Robust characteristics method for modelling multiphase visco-elasto-plastic thermo-mechanical problems, *Phys. Earth Planet. Inter.*, *163*, 83–105, doi:10.1016/j.pepi.2007.04.015.
- Gerya, T. (2010), *Introduction to Numerical Geodynamic Modelling*, Cambridge University Press, Cambridge, UK.
- Giordano, D., J. K. Russell, and D. B. Dingwell (2008), Viscosity of magmatic liquids: A model, *Earth Planet. Sci. Lett.*, *271*, 123–134, doi:10.1016/j.epsl.2008.03.038.
- Gudmundsson, A. (2006), How local stresses control magma-chamber ruptures, dyke injections, and eruptions in composite volcanoes, *Earth Sci. Rev.*, *79*, 1–31, doi:10.1016/j.earscirev.2006.06.006.
- Gudmundsson, A. (2011), Deflection of dykes into sills at discontinuities and magma-chamber formation, *Tectonophysics*, *500*, 50–64, doi:10.1016/j.tecto.2009.10.015.
- Hess, P. C. (1989), *Origin of Igneous Rocks*, Harvard University Press, Cambridge, MA.
- Hildreth, W., and S. Moorbath (1988), Crustal contributions to Arc magmatism in the Andes of central Chile, *Contrib. Mineral. Petrol.*, *98*(4), 455–489, doi:10.1007/BF00372365.
- Hirschmann, M. M. (2000), Mantle solidus: Experimental constraints and the effects of peridotite composition, *Geochem. Geophys. Geosyst.*, *1*, 10, 2000GC000070, doi:10.1029/2000GC000070.
- Hofmeister, A. M. (1999), Mantle values of thermal conductivity and the geotherm from phonon lifetimes, *Science*, *283*(5408), 1699–1706.
- Horsman, E., B. Tikoff, and S. Morgan (2005), Emplacement-related fabric and multiple sheets in the Maiden Creek sill, Henry Mountains, Utah, USA, *J. Struct. Geol.*, *27*, 1426–1444, doi:10.1016/j.jsg.2005.03.003.
- Huppert, H. E., and R. S. J. Sparks (1988), The generation of granitic magmas by intrusion of basalt into continental-crust, *J. Petrol.*, *29*(3), 599–624.
- Jellinek, A. M., R. C. Kerr, and R. W. Griffiths (1999), Mixing and compositional stratification produced by natural convection 1. Experiments and their application to Earth's core and mantle, *J. Geophys. Res.-Solid Earth*, *104*(B4), 7183–7201.
- Johannes, W. (1985), The petrology of granite, *Fortschritte Der Mineralogie*, *63*, 284–284.
- Kaizuka, S. (1992), Coastal evolution at a rapidly uplifting volcanic island: Iwo-Jima, Western Pacific Ocean, *Quaternary International*, *15*, 7–16.
- Kavanagh, J. L., T. Menand, and R. S. J. Sparks (2006), An experimental investigation of sill formation and propagation in layered elastic media, *Earth Planet. Sci. Lett.*, *245*, 799–813, doi:10.1016/j.epsl.2006.03.025.
- Kohlstedt, D. L., B. Evans, and S. J. Mackwell (1995), Strength of the lithosphere—Constraints imposed by laboratory experiments, *J. Geophys. Res.-Solid Earth*, *100*(B9), 17587–17602.
- Lavie, L. L., W. R. Buck, and A. N. B. Poliakov (2000), Factors controlling normal fault offset in an ideal brittle layer, *J. Geophys. Res.-Solid Earth*, *105*(B10), 23431–23442.
- Lee, C. T., R. L. Rudnick, and G. H. Brimhall (2001), Deep lithospheric dynamics beneath the Sierra Nevada during the Mesozoic and Cenozoic as inferred from xenolith petrology, *Geochem. Geophys. Geosyst.*, *2*, 2001GC000152, doi:10.1029/2001GC000152.
- Leuthold, J., O. Muntener, L. P. Baumgartner, B. Putlitz, M. Ovtcharova, and U. Schaltegger (2012), Time resolved

- construction of a bimodal laccolith (Torres Del Paine, Patagonia), *Earth Planet. Sci. Lett.*, *325*, 85–92, doi:10.1016/j.epsl.2012.01.032.
- Marsh, B. D. (1982), On the mechanics of igneous diapirism, stoping, and zone-melting, *Am. J. Sci.*, *282*(6), 808–855.
- MacLennan, J., and B. Lovell (2002), Control of regional Sea level by surface uplift and subsidence caused by magmatic underplating of Earth's crust, *Geology*, *30*(8), 675–678, doi:10.1130/0091-7613(2002)030<0675:CORSLB>2.0.CO;2.
- Mazzarini, F., G. Musumeci, D. Montanari, and G. Corti (2010), Relations between deformation and upper crustal magma emplacement in laboratory physical models, *Tectonophysics*, *484*, 139–146, doi:10.1016/j.tecto.2009.09.013.
- Menand, T. (2011), Physical controls and depth of emplacement of igneous bodies: A review, *Tectonophysics*, *500*, 11–19, doi:10.1016/j.tecto.2009.10.016.
- Menand, T., M. de Saint-Blanquat, and C. Annen (2011), Emplacement of magma pulses and growth of magma bodies preface, *Tectonophysics*, *500*, 1–2, doi:10.1016/j.tecto.2010.05.014.
- Michel, J., L. Baumgartner, B. Putlitz, U. Schaltegger, and M. Ovtcharova (2008), Incremental growth of the Patagonian Torres Del Paine laccolith over 90 K.Y., *Geology*, *36*, 459–462, doi:10.1130/G24546A.1.
- Olsen, S. N., B. D. Marsh, and L. P. Baumgartner (2004), Modelling Mid-crustal migmatite terrains as feeder zones for granite plutons: The competing dynamics of melt transfer by bulk versus porous flow, in *Special Paper 389: The Fifth Hutton Symposium on the Origin of Granites and Related Rocks*, edited, pp. 49–58, Geological Society of America.
- Petford, N. (1996), Dykes or diapirs?, *Trans. R. Soc. Edinb.-Earth Sci.*, *87*, 105–114.
- Petford, N., A. R. Cruden, K. J. W. McCaffrey, and J. L. Vigneresse (2000), Granite magma formation, transport and emplacement in the Earth's crust, *Nature*, *408*(6813), 669–673.
- Pickett, D. A., and J. B. Saleeby (1993), Thermobarometric constraints on the depth of exposure and conditions of plutonism and metamorphism at deep levels of the Sierra-Nevada batholith, Tehachapi Mountains, California, *J. Geophys. Res.-Solid Earth*, *98*(B1), 609–629.
- Pinkerton, H., and R. J. Stevenson (1992), Methods of determining the rheological properties of magmas at sub-liquidus temperatures, *J. Volcanol. Geotherm. Res.*, *53*(1–4), 47–66.
- Poli, S., and M. W. Schmidt (2002), Petrology of subducted slabs, *Annu. Rev. Earth Planet. Sci.*, *30*, 207–235, doi:10.1146/annurev.earth.30.091201.140550.
- Quick, J. E., S. Sinigoi, and A. Mayer (1994), Emplacement dynamics of a large mafic intrusion in the lower crust, Ivrea-Verbano zone, northern Italy, *J. Geophys. Res.*, *99*(B11), 21,559–521,573.
- Quick, J. E., S. Sinigoi, G. Peressini, G. Demarchi, J. L. Wooden, and A. Sbisà (2009), Magmatic plumbing of a large Permian caldera exposed to a depth of 25 km, *Geology*, *37*, 603–606, doi:10.1130/G30003A.1.
- Ranalli, G. (1995), *Rheology of the Earth*, Chapman & Hall, London.
- Riddick, S. N., and D. A. Schmidt (2011), Time-dependent changes in volcanic inflation rate near Three Sisters, Oregon, revealed by Insar, *Geochem. Geophys. Geosyst.*, *12*, Q12005, doi:10.1029/2011GC003826.
- Rudnick, R. (1990), Continental-crust-growing from below, *Nature*, *347*(6295), 711–712.
- Ruprecht, P., G. W. Bergantz, K. M. Cooper, and W. Hildreth (2012), The crustal magma storage system of Volcan Quizapu, Chile, and the effects of magma mixing on magma diversity, *J. Petrol.*, *53*, 801–840, doi:10.1093/ptrology/egs002.
- Schmeling, H., A. Y. Babeyko, A. Enns, C. Facenna, F. Funicello, T. Gerya, G. J. Golabek, S. Grigull, B. J. P. Kaus, G. Morra, S. M. Schmalholz, and J. van Hunen (2008), A benchmark comparison of spontaneous subduction models—Towards a free surface, *Phys. Earth Planet. Inter.*, *171*, doi:10.1016/j.pepi.2008.06.028.
- Schmidt, M. W., and S. Poli (1998), Experimentally based water budgets for dehydrating slabs and consequences for arc magma generation, *Earth Planet. Sci. Lett.*, *163* (1–4), 361–379.
- Sinigoi, S., J. E. Quick, G. Demarchi, and U. Klotzli (2011), The role of crustal fertility in the generation of large silicic magmatic systems triggered by intrusion of mantle magma in the deep crust, *Contrib. Mineral. Petrol.*, *162*, 691–707, doi:10.1007/s00410-011-0619-2.
- Sobolev, S. V., and A. Y. Babeyko (2005), What drives orogeny in the Andes?, *Geology*, *33*, 617–620, doi:10.1130/G21557.
- Sparks, R. S. J., and L. A. Marshall (1986), Thermal and mechanical constraints on mixing between mafic and silicic magmas, *J. Volcanol. Geotherm. Res.*, *29*(1–4), 99–124.
- Spiegelman, M., P. B. Kelemen, and E. Aharonov (2001), Causes and consequences of flow organization during melt transport: The reaction infiltration instability in compactible media, *J. Geophys. Res.-Solid Earth*, *106* (B2), 2061–2077.
- Stern, R. J. (2002), Subduction zones, *Rev. Geophys.*, *40*(4), 1012, doi:10.1029/2001RG000108.
- Tarasewicz, J., R. S. White, A. W. Woods, B. Brandsdottir, and M. T. Gudmundsson (2012), Magma mobilization by downward-propagating decompression of the Eyjafjallajökull volcanic plumbing system, *Geophys. Res. Lett.*, *39*, L19309, doi:10.1029/2012GL053518.
- Thompson, A. B., and J. A. D. Connolly (1995), Melting of the continental-crust—Some thermal and petrological constraints on anatexis in continental collision zones and other tectonic settings, *J. Geophys. Res.-Solid Earth*, *100*(B8), 15565–15579.
- Turcotte, D. L., and G. Schubert (2002), *Geodynamics*, Cambridge University Press, Cambridge, UK.
- Turner, S., and F. Costa (2007), Measuring timescales of magmatic evolution, *Elements*, *3*, 267–272, doi:10.2113/gselements.3.4.267.
- Vogt, K., T. V. Gerya, and A. Castro (2012), Crustal growth at active continental margins: Numerical modeling, *Phys. Earth Planet. Inter.*, *192*, 1–20, doi:10.1016/j.pepi.2011.12.003.
- Zellmer, G. F., and C. Annen (2008), An introduction to magma dynamics, in *Dynamics of Crustal Magma Transfer, Storage and Differentiation*, edited by C. Annen, and G. F. Zellmer, Geological Society (London) Special Publications, *304*, pp. 1–13, doi:10.1144/SP304.1.